Interplay of metallicity, ferroelectricity, and layer charges in $SmNiO_3/BaTiO_3$ superlattices

Edith Simmen* and Nicola A. Spaldin
Materials Theory, ETH Zurich, 8093 Zurich, Switzerland

(Received 15 November 2024; accepted 18 March 2025; published 11 April 2025)

Using density-functional theory, we demonstrate that the formal layer charges of the metallic samarium nickelate electrode influence the spontaneous ferroelectric polarization of the barium titanate in $SmNiO_3/BaTiO_3$ capacitors. We find that, despite the metallic screening of $SmNiO_3$, the spontaneous polarization of $BaTiO_3$ always aligns with the layer polarization of the $SmNiO_3$ formal charges. We also find zero critical thickness for the ferroelectricity in $BaTiO_3$ in this orientation. The opposite polarization direction is highly disfavored for thin $BaTiO_3$ slabs but becomes less unstable with increasing slab thickness. We construct a simple electrostatic model that allows us both to study the behavior for thicker $BaTiO_3$ and $SmNiO_3$ slabs and to extract the influence of various material parameters on the behavior. We mimic a metal-insulator transition in the $SmNiO_3$ by varying the metallic screening length, which we find influences the stability of the ferroelectric polarization. Our results show that layer charges in the metal electrodes strongly influence the properties of ferroelectric capacitors and can even provide new ways to control them.

DOI: 10.1103/PhysRevResearch.7.023044

I. INTRODUCTION

Thin-film ferroelectrics are a subject of active research both because of their fundamental interest and for their potential applications in low-energy electronic technologies [1–4], such as ferroelectric tunnel junctions [1,3] or field-effect devices [3]. For most of these applications, the ferroelectric films are grown in a capacitor geometry with metallic electrodes. The electrode is needed to control or read out the ferroelectric state [2] and to screen interface charges that accumulate due to the spontaneous polarization $\mathbf{P}_{\text{spont}}$ of the ferroelectric film. In the absence of such screening, these interface charges lead to a depolarizing field that counteracts and suppresses the polarization [5].

While perovskite oxide metals provide good coherence with perovskite ferroelectrics, they can contain formally positively or negatively charged sublayers of ions. For example, the formally +3 charges of the A- and B-site cations in the rare-earth nickelates $RNiO_3$ lead to a metallic phase with charged (001) RO^+ and NiO_2^- sublayers. In their insulating states, these layer charges would lead to a polar discontinuity at the interface to a material with no or different layer charges [6]. Such a polar discontinuity has been studied in detail in the ferroelectric III-III perovskite $BiFeO_3$, both at the surface [7] and at the interface to the II-IV $SrRuO_3$ electrode [8,9]. The resulting polar discontinuity strongly favors one of the two polarization directions [8]. The polarization direction minimizing the interface charges, referred to as the happy polarization [7], is much lower in energy than the opposite, unhappy polarization which increases the interface charges. In the metallic state of the rare-earth nickelates, the additional metallic screening could reduce or erase the effects of this polar discontinuity.

The interface charge σ_{inter} resulting from the polar discontinuity between two different materials is determined by the bulk polarizations $\mathbf{P}_{\text{bulk},n}$ of the two materials n forming the interface

$$\sigma_{\text{inter}} = (\mathbf{P}_{\text{bulk},1} - \mathbf{P}_{\text{bulk},2}) \times \hat{n}, \tag{1}$$

where $\hat{n}$ is the surface normal [6]. In addition to the spontaneous polarization, the layer polarization $\mathbf{P}_{\text{layer}}$ caused by the charged sublayers also contributes to the bulk polarization, so that

$$\mathbf{P}_{\text{bulk},n} = \mathbf{P}_{\text{spont},n} + \mathbf{P}_{\text{layer},n}. \tag{2}$$

$\mathbf{P}_{\text{spont}}$ is the change in bulk polarization relative to a centrosymmetric reference structure and is non-zero only if inversion symmetry is broken. $\mathbf{P}_{\text{layer}}$ can be calculated by summing the formal charges Z_i times the positions $\mathbf{r}_i$ of all atoms i in the unit cell of volume Ω, $\frac{e}{\Omega}\sum_i \mathbf{r}_i \times Z_i$ [6]. In the case of a II-IV perovskite, $\mathbf{P}_{\text{layer}}$ is $0\,\mu\text{C}\,\text{cm}^{-2}$ modulo the polarization quantum $\mathbf{P}_q$ and for a flat (001) surface, the relevant value to use for $\mathbf{P}_{\text{layer}}$ in Eq. (2) is $0\,\mu\text{C}\,\text{cm}^{-2}$.

Figure 1(a) illustrates the (001) interface between a representative III-III ($SmNiO_3$) and a II-IV ($BaTiO_3$) perovskite material. For centrosymmetric $SmNiO_3$, the normal component of $\mathbf{P}_{\text{spont}}$ is $0\,\mu\text{C}\,\text{cm}^{-2}$ and the layer polarization in the configuration of Fig. 1 is approximately $+50\,\mu\text{C}\,\text{cm}^{-2}$ (upper arrow) so that, considering the opposite surface normals, the NiO_2^- and SmO^+ surface have a respective charge of $\sim -50\,\mu\text{C}\,\text{cm}^{-2}$ and $\sim +50\,\mu\text{C}\,\text{cm}^{-2}$.

*Contact author: edith.simmen@mat.ethz.ch

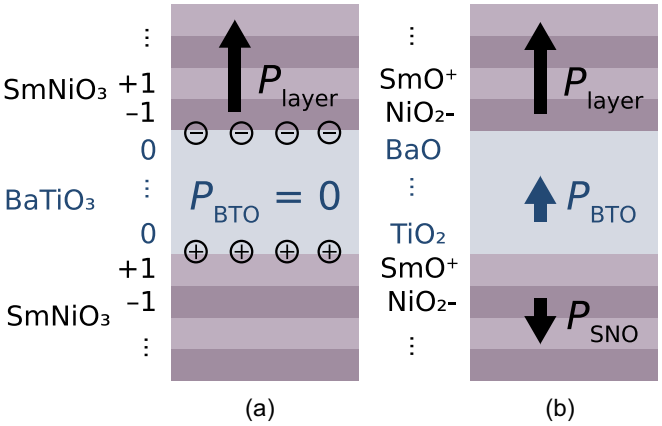

FIG. 1. Illustration of the polar discontinuity resulting from the formal layer charges in $SmNiO_3/BaTiO_3$ superlattices. (a) Paralectric $BaTiO_3$. The charged sublayers of ± 1 electron charge per formula unit lead to a non-zero normal component of the layer polarization P_{layer} in III-III $SmNiO_3$ and a net positive or negative charge at its interface with the II-IV $BaTiO_3$. (b) Ferroelectric $BaTiO_3$ in the happy orientation. The interface charges are partially compensated when the normal component of the spontaneous polarization P_{BTO} in $BaTiO_3$ aligns with and/or the normal component of the polar displacements P_{SNO} of $SmNiO_3$ develop opposite to P_{layer}.

For paraelectric $BaTiO_3$ [Fig. 1(a)], both spontaneous polarization ($\mathbf{P}_{\text{BTO}}$) and layer polarization are zero, giving zero bulk polarization and surface charges. As a result, we find $\sigma_{\text{inter}} = -50\,\mu\text{C}\,\text{cm}^{-2}$ and $+50\,\mu\text{C}\,\text{cm}^{-2}$ for the upper NiO_2/BaO and lower SmO/TiO_2 interfaces, respectively.

If the spontaneous polarization in either material is nonzero, the interface charge will change accordingly. If the orientation of the spontaneous polarization in either or both of the materials causes a reduction of the interface charge then the polar discontinuity will be (partially) compensated. We refer to this situation as ionic screening, to distinguish it from metallic screening associated with the metallicity of the electrode. Such compensation is achieved if the spontaneous polarization in the $BaTiO_3$ aligns with the layer polarization (middle arrow in Fig. 1(b)) and/or if a spontaneous polarization forms inside the $SmNiO_3$ opposite to the layer polarization (bottom arrow). Interface charges increase when the direction of the spontaneous polarization in either material is reversed. For a detailed discussion of the interface charges between III-III and II-IV perovskites, see Ref. [8].

Here, we perform a detailed study of the role of layer charges at the ferroelectric-metallic interface in capacitors for which the ferroelectric has uncharged sublayers and the metallic electrodes contain formally charged sublayers. We choose the prototypical perovskite ferroelectric $BaTiO_3$, with its polar, tetragonal phase at room temperature [10], for our ferroelectric material. For our metallic electrode, we choose orthorhombic perovskite $SmNiO_3$, which has *Pbnm* symmetry [11] and NiO_6 octahedral rotations corresponding to the Glazer notation $a^-a^-c^+$. Since we are interested in the interplay between metallicity and layer charges, we focus on the metallic phase of $SmNiO_3$, noting that, like most members of the rare-earth nickelate family, it undergoes a sharp transition to an insulating phase on cooling. Importantly for practical applications, the metal-insulator transition (MIT) in $SmNiO_3$ occurs just above room temperature (400 K [12]).

The effect of layer polarization within metal electrodes on ferroelectric capacitors has been touched on in the literature, for the cases of $LaNiO_3$ [13–15] and $La_{1-x}Sr_xMnO_3$ (LSMO) [9]. In Ref. [13], a preferred polarization direction for $BaTiO_3$ was identified in density-functional theory (DFT) calculations of asymmetric $LaNiO_3/BaTiO_3/LaNiO_3$ heterostructures due to the polar discontinuity. In symmetric $LaNiO_3/BaTiO_3$ superlattices, Ref. [14] used DFT to identify improved screening of the polar discontinuity at the NiO_2^-/BaO interface compared to the SmO^+/TiO_2 interface, leading to stronger ferroelectricity at low thicknesses. While the internal field due to the polar discontinuity was estimated to be negligibly small compared to the experimental coercive voltages in $LaNiO_3$/PZT heterostructures [15], Ref. [9] measured a shift in the hysteresis loop of PZT-LSMO heterostructures consistent with the polar discontinuity. An in-depth DFT study on the effect of layer charges within the metallic electrode in asymmetric superlattices is, however, missing.

We start by investigating the effect of the polar discontinuity resulting from the difference in sublayer charges between $BaTiO_3$ and $SmNiO_3$ on the spontaneous polarization in $BaTiO_3$ using DFT. We confirm that the spontaneous polarization in such superlattices, with charged sublayers within the metallic electrode, shows a clear preference for the happy orientation and is not switchable for thin slabs. In addition, we find the absence of a critical thickness in $BaTiO_3$ for the polarization orientation minimizing the interface charges. Using an electrostatic model, we next study the polar discontinuity in thicker slabs and examine the effects of the dielectric permittivity and the metallic screening length on the system. As expected, we find that as the slab thickness increases, the unhappy orientation becomes less unstable. Lastly, we show that the effect of the polar discontinuity on the ferroelectric is reduced for a smaller effective metallic screening length and a higher dielectric constant, providing a route to tuning the ferroelectric properties for different applications.

II. METHODS

We calculated the properties of superlattices of $BaTiO_3$ and $SmNiO_3$ using DFT as implemented in the VASP Code [16,17]. We described the exchange-correlation with the Perdew-Burke-Ernzerhof functional revised for solids [18]. Projector augmented-wave pseudopotentials [19,20] were used with the following valence electrons (name of VASP pseudopotential): $5s^25p^66s^2$ (Ba_sv), $3p^64s^23d^4$ (Ti_sv), $2s^22p^4$ (O), $3p^64s^23d^8$ (Ni_pv) and $5s^25p^66s^25d^1$ (Sm_3), with the f electrons of Sm frozen into the core. In-plane, the superlattices were constructed from supercells of 1×1 formula units when the rotations in $SmNiO_3$ were disabled [Fig. 2(b)] and from supercells of $\sqrt{2} \times \sqrt{2}$ formula units when they were allowed [Fig. 4(b)]. Out-of-plane, the superlattices were constructed from layers of five $BaTiO_3$ and four $SmNiO_3$ formula units unless stated otherwise. To model a $SrTiO_3$ substrate, which is commonly used in similar experimental heterostructures [8,9,15,21], we constrained the in-plane lattice parameters to those of cubic $SrTiO_3$. We used $a = 3.898$ Å from the DFT

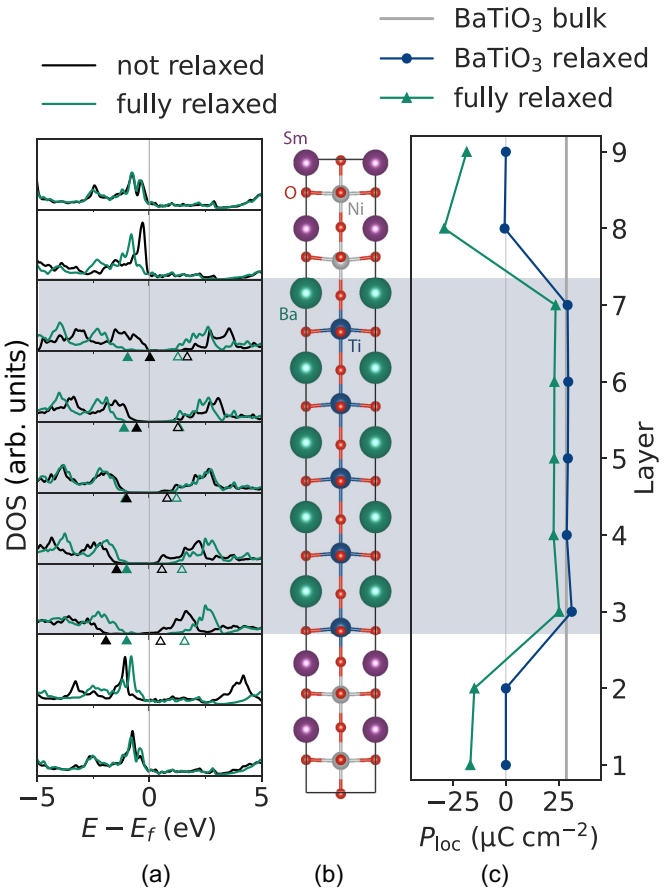

FIG. 2. Superlattice without rotations in $SmNiO_3$: (a) Layer-by-layer DOS for superlattice without (black) and with (green) relaxation. The band shift in $BaTiO_3$ is indicated by corresponding black and green triangles for the valence band maximum (full) and conduction band minimum (empty). (b) Structure of the superlattice after full relaxation. (c) Layer-resolved local polarization ($\mu C\,cm^{-2}$) with only the $BaTiO_3$ layer relaxed (blue) and with relaxation of the full structure (green). The polarization value of bulk $BaTiO_3$ from Eq. (3) (vertical gray line) is shown as a reference.

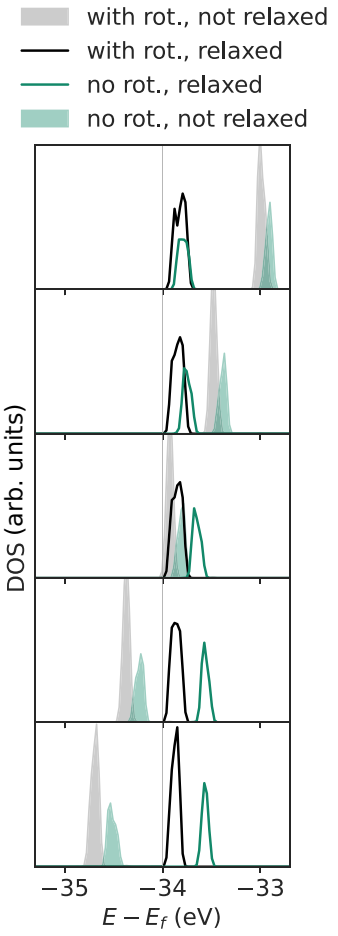

FIG. 3. Layer-resolved DOS for $BaTiO_3$ core states for superlattice with active (black) and disabled (green) rotations that were either not relaxed (area) or fully relaxed (line).

calculations in Ref. [22], resulting in $-2.2\,\%$ compressive and $3.8\,\%$ tensile strain compared to our relaxed bulk $BaTiO_3$ and $SmNiO_3$ unit cells, respectively. The c-axis vector was allowed to relax to its lowest energy value. We used an energy cutoff of 650 eV and the structure was relaxed until the forces on the atoms were less than $0.01\,eV\text{Å}^{-1}$. We employed $8\times8\times1$ and $16\times16\times1$ Monkhorst-Pack k-point grids [23] during relaxations for superlattices with active and disabled rotations in $SmNiO_3$ respectively, and for density-of-states (DOS) calculations, the k-point grid was doubled in-plane. We compute the layer-resolved DOSs by summing the projected DOSs on all the atoms in each unit cell-thick layer.

The relaxations of the happy superlattices were performed in two steps: first, we relaxed only $SmNiO_3$ while fixing $BaTiO_3$ to its high-symmetry cubic reference structure, and next, we relaxed all atoms in the superlattice. For the unhappy relaxations, three layers of $BaTiO_3$ were fixed to the bulk oppositely polarized structure.

We evaluated the c-axis component of the local spontaneous polarization resolved by layers by summing the products of the formal charges Z and the displacements Δd from their centrosymmetric position along the c axis over all ions i in the layer according to

$$P_{\text{loc}} = \frac{e}{\Omega}\sum_i \Delta d_i \times Z_i, \tag{3}$$

with e and Ω being the elementary charge and the volume of the corresponding layer, respectively. The height of one layer corresponds to the distance from one A atom (A = Ba, Sm) to the next, equivalent to the height of one formula unit along the c axis. To quantify polar displacements in metallic $SmNiO_3$, we also calculated the ionic off-centering using Eq. (3), recognizing that the resulting quantity is not a true polarization because of the metallicity. The analogous summation according to Eq. (3) in bulk $BaTiO_3$ with the in-plane lattice parameters set to those of $SrTiO_3$ yields a spontaneous polarization of $P_{BaTiO_3} = 28.6\,\mu C\,cm^{-2}$ along the c axis. In comparison, a Berry phase calculation [24,25] for the same bulk $BaTiO_3$ unit cell gives a spontaneous polarization of $44.6\,\mu C\,cm^{-2}$. While using formal charges generally underestimates the spontaneous polarization in $BaTiO_3$, it provides a consistent method for estimating the contribution of polar displacements in both $SmNiO_3$ and $BaTiO_3$ to the interface charge. The spontaneous polarizations

of bulk $BaTiO_3$ or $SmNiO_3$ reported for example in Fig. 8 are calculated analogously to Eq. (3) using formal charges.

Phonon frequencies at the Γ point were calculated using five-atom $BaTiO_3$ and 20-atom $SmNiO_3$ unit cells with the atomate2 [26] phonon workflow, and any post-processing was done using phonopy [27,28].

III. RESULTS

A. Properties of superlattices with $SmNiO_3$ rotations disabled

We start by investigating simplified superlattices with the octahedral rotations of $SmNiO_3$ disabled. Our motivation for studying this simplified structure is twofold: First, fewer in-plane unit cells are needed, thus reducing the computational time. Second, previous studies on similar superlattices with $LaNiO_3$ and $BaTiO_3$ [29] or $PbTiO_3$ [15,30] have focused on superlattices with disabled octahedral rotations. By doing the same, we can both compare our results to literature and validate this approximation.

We begin by calculating the layer-resolved DOS of $(BaTiO_3)_5(SmNiO_3)_4$ (one layer corresponds to the height of one perovskite formula unit) with both $BaTiO_3$ and $SmNiO_3$ constrained to the high-symmetry cubic perovskite structure. Figure 2(a) shows the results in black with SmO/TiO_2 as the lower and NiO_2/BaO as the upper interface in the superlattice [as illustrated in Fig. 1(a)]. We note a clear shift of the $BaTiO_3$ bands to higher energies (black triangles) when going from the lowest to the highest $BaTiO_3$ layer, indicating the presence of an electric field inside the $BaTiO_3$ layer. We can assign the origin of this electric field to the polar discontinuity and the resulting charges at the interface between $SmNiO_3$ and $BaTiO_3$. We conclude that, despite being metallic, $SmNiO_3$ cannot fully screen these interface charges.

Next, we relax the structure. We find that, as expected, the $BaTiO_3$ slab develops a spontaneous polarization. The corresponding displacements of Ti with respect to O atoms are visible in Fig. 2(b), and in Fig. 2(c) we show the resulting local polarization calculated using Eq. (3). First, we relax only the $BaTiO_3$ slab and $BaTiO_3$ develops a formal-charge polarization of $29\,\mu C\,cm^{-2}$ (blue line in Fig. 2), equal to its bulk formal-charge value (gray line). The spontaneous polarization in the $BaTiO_3$ slab aligns with the layer polarization in $SmNiO_3$ to compensate the polar discontinuity. Note that, since the spontaneous polarization of bulk $BaTiO_3$ from a Berry phase calculation at this in-plane lattice constant is $44.6\,\mu C\,cm^{-2}$, the $BaTiO_3$ almost entirely compensates the $\sim 50\mu C\,cm^{-2}$ polar discontinuity. Next, we relax the full superlattice. We find that in this case, $SmNiO_3$ develops polar displacements of $-18\,\mu C\,cm^{-2}$ opposite to its layer polarization, reducing its bulk polarization, so that the spontaneous polarization in $BaTiO_3$ reduces to $23\,\mu C\,cm^{-2}$ (green line). The band bending due to the polar discontinuity disappears upon relaxation [green in Fig. 2(a)].

We can estimate the remaining uncompensated interface charges using Eq. (1) and the normal components of the spontaneous polarizations P_{BTO} for the $BaTiO_3$ and P_{SNO} for the $SmNiO_3$ slabs (obtained by averaging the local polarizations with the interfacial layers excluded):

$$\sigma_{inter} = 50\,\mu C\,cm^{-2} + P_{BTO} - P_{SNO.} \quad (4)$$

We find that relaxation of the ions considerably reduces σ_{inter} from $\pm 50\,\mu C\,cm^{-2}$ to values of only $\pm 10\,\mu C\,cm^{-2}$. Note that Eq. (4) likely overestimates the amount of interface charge because the true polarization of $BaTiO_3$ is higher than the value obtained from Eq. (3).

This means that the amount of interfacial charge that the metallic carriers need to screen to result in the observed zero band bending is likely less than $\pm 10\,\mu C\,cm^{-2}$. The metallic screening is also considerably less than the $-18\,\mu C\,cm^{-2}$ screened by the polar displacements of the ions.

Similarly, Ref. [31] reported that polar displacements over 2–3 formula units in the $SrRuO_3$ electrode of $BaTiO_3/SrRuO_3$ superlattices helped to stabilize a larger ferroelectric polarization in the $BaTiO_3$. In contrast to their findings, the polar displacements in our superlattice are uniform across the entire $SmNiO_3$ slab, although it is unclear whether the polar displacements would remain uniform for thicker slabs.

Interestingly, in the relaxed structure, we find a small band bending in the $BaTiO_3$ core states opposite to the field introduced by the layer charges, see Fig. 3. We assign the inverse field to increased polar displacements in the $SmNiO_3$ slab at the BaO/NiO_2 interface due to the change in A-cation size and charge across the interface. NiO_2^- at this interface is sandwiched between a sublayer with large Ba^{2+} and small Sm^{3+} ions which induce an off-centering of O^{2-} relative to Ni^{3+} towards Sm^{3+}. Additionally, the O^{2-} are more electrostatically attracted to the Sm^{3+} than the Ba^{2+} further enhancing the local interfacial polar displacement. The enhanced polar displacement in NiO_2 at this interface likely causes the rest of the $SmNiO_3$ to follow suit, overcompensating for the polar discontinuity and leading to an inverse band bending. In $BaTiO_3/SrRuO_3$ superlattices, an analogous enhancement of the spontaneous polarization in the first two RuO_2 sublayers due to the ion size difference at the BaO/RuO_2 interface has been observed [32]. We will determine in the next section whether this effect is inherent to the superlattice or if it is a consequence of disabling the rotations in the $SmNiO_3$.

In conclusion, we find that in the absence of a spontaneous polarization in the $BaTiO_3$, clear signatures of an electric field across the $BaTiO_3$ slab are present in the calculated electronic structure, indicating the incomplete screening of the polar discontinuity by the metallic $SmNiO_3$. σ_{inter} is strongly reduced by the spontaneous polarization in $BaTiO_3$ aligning parallel to the layer polarization within $SmNiO_3$, along with additional opposite polar displacements in $SmNiO_3$.

B. Properties of superlattices with active rotations in $SmNiO_3$

We continue by comparing our previous results to the case in which $SmNiO_3$ is allowed to develop octahedral rotations. While the polar discontinuity from the layer polarization remains unaffected by the introduction of octahedral rotations (the formal charge state is the same for $SmNiO_3$ with active and disabled rotations), the metallic screening of the $SmNiO_3$ electrode and the ionic screening in $SmNiO_3$ and $BaTiO_3$ may be affected. We again find a band bending in the layer-resolved DOS if we do not relax our superlattice and constrain $BaTiO_3$ to the cubic symmetry [Fig. 4(a) in black]. The core states in Fig. 3 show a band bending with the same slope as for the superlattice with disabled rotations and we thus conclude

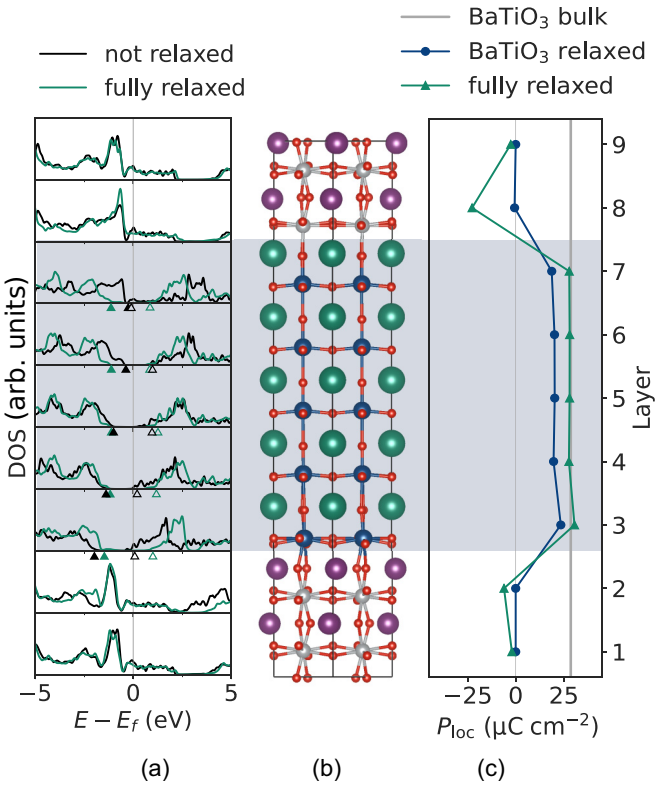

FIG. 4. Superlattice with rotations in $SmNiO_3$: (a) Layer-by-layer DOS for superlattice without (black) and with (green) relaxation. The band shift in $BaTiO_3$ is indicated by corresponding green and black triangles for the valence band maximum (full) and conduction band minimum (empty). (b) Superlattice after full relaxation. (c) Layer-resolved, local polarization ($\mu C\,cm^{-2}$) with only the $BaTiO_3$ relaxed (blue) and relaxation of the full structure (green). The spontaneous polarization value of bulk $BaTiO_3$ strained to $SrTiO_3$ (vertical gray line) is shown as a reference.

that the metallic screening is the same for both cases. As for the case of disabled rotations, the band bending disappears once we fully relax the structure [green in Fig. 4(a)], and a spontaneous polarization forms in $BaTiO_3$ aligned with the layer polarization of $SmNiO_3$. The corresponding polar displacements of Ti and O are clearly visible in Fig. 4(b). We again relax first only the $BaTiO_3$ slab with $SmNiO_3$ fixed [blue line in Fig. 4(c)] and the full structure in a second step (green line). The spontaneous polarization in the $BaTiO_3$ slab is $20\,\mu C\,cm^{-2}$ after relaxation of the $BaTiO_3$ slab and upon full relaxation, it increases to a spontaneous polarization of $28\,\mu C\,cm^{-2}$, which is very close to the formal-charge spontaneous polarization of $29\,\mu C\,cm^{-2}$ in bulk $BaTiO_3$. Overall, the response of $BaTiO_3$ to the polar discontinuity in superlattices with rotations in the $SmNiO_3$ is analogous to that in the superlattice with disabled rotations.

The octahedral rotations, however, clearly influence the polar displacements in $SmNiO_3$: We find that the average polar displacement of the $SmNiO_3$ slab reduces from $-18\,\mu C\,cm^{-2}$ in superlattices with disabled rotations to $-2\,\mu C\,cm^{-2}$ in superlattices with active octahedral rotations. In the latter structure, the local polar displacement is largest at the upper NiO_2/BaO interface where the octahedral rotations are more suppressed [see Fig. 4(b)], however, in contrast to the superlattices with disabled rotations, the rest of the $SmNiO_3$ does not form any considerable polar displacements. We confirm this behavior by calculating the frequency of the lowest polar phonon mode leading to the out-of-plane polar displacement in bulk $SmNiO_3$ with active and disabled rotations. The behavior we find in the superlattice is consistent with the hardening of the polar mode, i.e., the increase of the bulk phonon frequencies, from $\sim -20\,cm^{-1}$ to $175\,cm^{-1}$ on the introduction of the octahedral rotations (see Fig. 8). The presence of rotations in $SmNiO_3$ highly disfavors the formation of polar displacements. Octahedral rotations and ferroelectricity are known to often not coexist and several studies have shown that if the rotations are suppressed, ferroelectricity may emerge in perovskites that are otherwise not ferroelectric [33–35]. Additionally, the steric effects that suppress the rotations at the NiO_2/BaO interface enhance the polar displacements, analogous to the effect we observed in superlattices with disabled rotations.

We have thus shown that the polar discontinuity arising from $SmNiO_3$ with active rotations results in a similar $BaTiO_3$ polarization as in the superlattice with $SmNiO_3$ rotations disabled and that the contribution of the metallic screening to reducing σ_{inter} is similar for $SmNiO_3$ with and without rotations. While the behavior in $BaTiO_3$ is similar in the two cases, ionic screening in $SmNiO_3$ is reduced when rotations are active, and consequently, the interface charges of $\pm 20\,\mu C\,cm^{-2}$ are higher.

C. Stability of the polar displacements

In this section, we explore two aspects of the stability of the ferroelectricity in $BaTiO_3$: first, the critical thickness of the spontaneous polarization for $BaTiO_3$ and second, the stability of the unhappy polarization orientation with increasing $BaTiO_3$ slab thickness.

We begin by calculating the energy as a function of the bulk soft mode distortion for superlattices containing one, five, and ten layers of $BaTiO_3$ and four layers of $SmNiO_3$. Our results are shown in Fig. 5(a). The soft mode distortion is defined to be the change in structure of bulk $BaTiO_3$ between the high-symmetry cubic and the polar tetragonal phase. A distortion of 0 thereby corresponds to cubic $BaTiO_3$ and in the fully polarized bulk $BaTiO_3$ structure, the distortion is 1. The superlattices were then constructed from a slab of $BaTiO_3$ with different fractional soft-mode distortions and a slab of $SmNiO_3$ with active rotations, and the energy was calculated without any further structural relaxation.

We first analyze the right-hand side of Fig. 5(a), which shows the energy as a function of soft mode distortion in the happy direction. We find a global minimum at +1 soft mode distortion for all three thicknesses down to 1 layer of $BaTiO_3$, indicating that these superlattices have no critical thickness. Next, we construct superlattices with 1–5 layers of centrosymmetric $BaTiO_3$ and four layers of $SmNiO_3$ with active rotations and subsequently relax them. Figure 6 shows the averaged local polarization of the $BaTiO_3$ slab, P_{BTO}, (green) as a function of slab thickness. We indeed find that the spontaneous polarization of the $BaTiO_3$ slab is stable down to a single unit cell and maintains a polarization value close

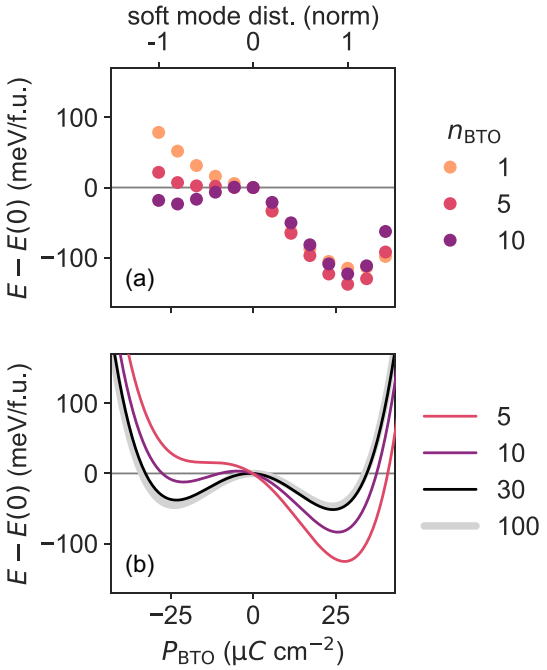

FIG. 5. Energy as a function of the frozen-in spontaneous polarization for different $BaTiO_3$ slab thicknesses. The energy is normalized by the total number of layers in the superlattice including that of $SmNiO_3$. The polar displacements of $SmNiO_3$ are constrained to zero and the energy zero is set to that of the superlattice with zero $BaTiO_3$ polarization. (a) Energy profile obtained from DFT for $SmNiO_3/BaTiO_3$ superlattices with active rotations in the 4 $SmNiO_3$ layers and $n_{BTO} = 1, 5, 10$ $BaTiO_3$ layers. (b) Energy profile obtained from the electrostatic model for superlattices $n_{BTO} = n_{SNO} = 5, 10, 30, 100$ layers. Note that the minimum in a) is at a higher formal-charge polarization ($P_{BTO} = 28.6\,\mu C\,cm^{-2}$) compared to (b) ($P_{BTO} = 24.0\,\mu C\,cm^{-2}$).

to that of bulk $BaTiO_3$ (grey dashed line). This is in striking contrast to the critical thickness of six unit cells found in $BaTiO_3$ with $SrRuO_3$ electrodes which do not contain charged (001) layers [36]. Our findings are consistent with Ref. [13], which reported an absence of critical thickness for $BaTiO_3/LaNiO_3$ superlattices, and indicate a strong polarizing field created by the interface charges [37].

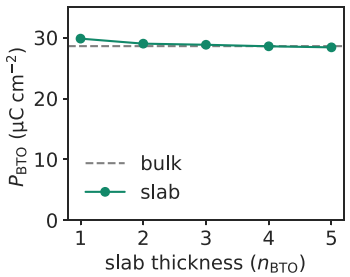

FIG. 6. Spontaneous polarization of the $BaTiO_3$ slab P_{BTO} as a function of $BaTiO_3$ slab thickness in $(BaTiO_3)_n(SmNiO_3)_4$ superlattices in the happy orientation. Note that in this case, the interface layers were included when calculating P_{BTO}. The formal-charge spontaneous polarization value of bulk $BaTiO_3$ is given as a reference (gray dashed line).

Next, we focus on the left-hand side of Fig. 5(a) which corresponds to the unhappy polarization direction where P_{loc} of $BaTiO_3$ is opposite to P_{layer} of $SmNiO_3$. Without any metallic screening, the polar discontinuity in the unhappy orientation would increase up to $\sim\pm 80\,\mu C\,cm^{-2}$ for P_{loc} of $BaTiO_3$ equal to the formal-charge polarization of bulk $BaTiO_3$. Hence, we would expect this orientation to be energetically highly disfavored, particularly for very thin $BaTiO_3$ slabs. In previous studies of $BiFeO_3/SrRuO_3$ superlattices, for example, the unhappy polarization orientation of $BiFeO_3$ was metastable only for six or more $BiFeO_3$ layers [8] and a similar study for $BaTiO_3/LaNiO_3$ superlattices found that the disfavored orientation could only be stabilized for more than eight $BaTiO_3$ layers [13].

For five layers of $BaTiO_3$, we find no metastable minimum for the unhappy orientation. For thicker layers, a local minimum that is ~ 100 meV/f.u. higher in energy than the global minimum, is found. Therefore, for a large enough number of $BaTiO_3$ layers, we expect a metastable unhappy state and switchable $BaTiO_3$ polarization albeit with a strong exchange bias. Note that the energy minimum for the unhappy orientation appears at -0.8 soft mode distortion, suggesting that we should expect a smaller spontaneous polarization in this orientation.

We find that superlattices with less than ten layers of $BaTiO_3$ initialized in the unhappy orientation always reverse the orientation of the $BaTiO_3$ polarization upon relaxation, resulting in the happy state. We are able to study the unhappy system, however, by fixing the middle three layers of $BaTiO_3$ to $-P_{spont}$ and relaxing the remaining atoms. The resulting DOS for the superlattice with rotations [purple in Fig. 7(a)] shows a similar although stronger band bending to that of the unrelaxed superlattices with centrosymmetric $BaTiO_3$ (black in Figs. 2 and 4). The band bending is strong enough to shift the conduction band of the $BaTiO_3$ below the Fermi level at the lower TiO_2/SmO interface, indicating an additional screening mechanism of electrons in the interfacial $BaTiO_3$ layer. The results for $SmNiO_3$ with disabled rotations are similar (Fig. 11).

The structures of both $SmNiO_3$ and $BaTiO_3$ are affected by the increased polar discontinuity in the unhappy state. $BaTiO_3$ reduces its local polarization at the interfaces where the atoms are not constrained [Fig. 7(c)] and, despite the rotations, $SmNiO_3$ increases its polar displacements.

In conclusion, we find the unhappy orientation of $BaTiO_3$ in $SmNiO_3/BaTiO_3$ superlattices to be energetically highly disfavored, and we are only able to stabilize the metastable unhappy orientation for ten layers or more of $BaTiO_3$. The happy orientation, however, shows a clear stable minimum for all slab thicknesses, allowing an out-of-plane polarization down to a single unit cell with no critical thickness.

D. Electrostatic model

In this last section, we construct an electrostatic model and use it to study the stability of the two polarization states for thick layers with up to 100 unit cells of $BaTiO_3$ and $SmNiO_3$ each, which are not accessible within DFT. We also use it to determine the effect of various parameters such as the dielectric permittivity and the effective screening length

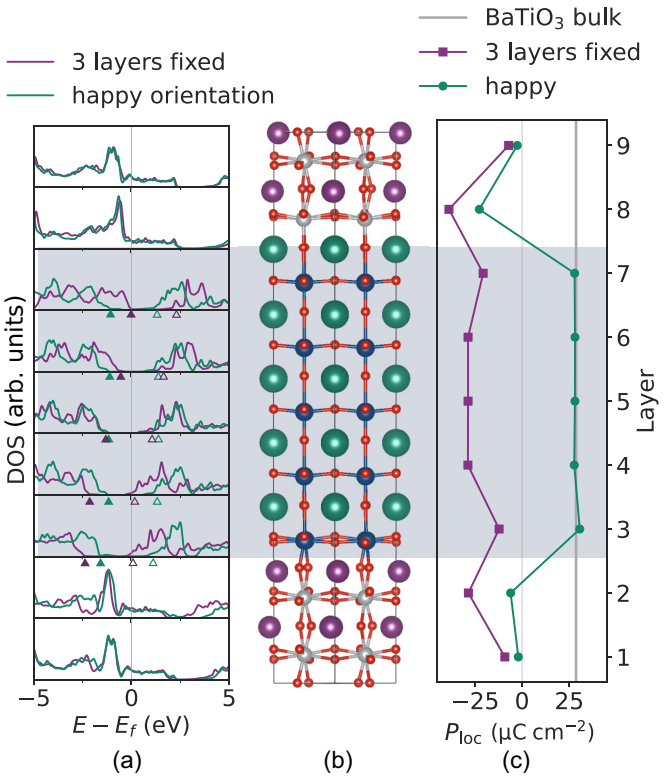

FIG. 7. Unhappy superlattice with three fixed $BaTiO_3$ layers: (a) Local DOS of superlattice with three $BaTiO_3$ layers fixed to the unhappy orientation (purple) and the happy superlattice from Fig. 4 (green). The band shift in $BaTiO_3$ is indicated by corresponding green and purple triangles for the valence band maximum (full) and conduction band minimum (empty). (b) Superlattice after relaxation with three fixed layers. (c) Layer-resolved, local polarization ($\mu C\,cm^{-2}$) for relaxation with the unhappy, fixed $BaTiO_3$ layers (purple) and the relaxed happy structure from Fig. 4 (green).

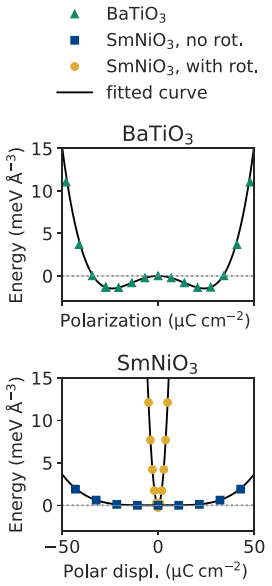

FIG. 8. Calculated energy as a function of polarization as obtained from freezing in the lowest polar phonon mode for bulk $BaTiO_3$ (upper panel) and bulk $SmNiO_3$ with active (circles) and disabled (squares) rotations (lower panel) and in-plane lattice constants strained to $SrTiO_3$. The spontaneous polarization is calculated analogously to Eq. (3) using formal charges. The curve obtained from fitting Eq. (B2) is shown in black.

on the behavior to guide possible choices of materials for future work.

The model describes the electrostatics at the interface and the associated energy costs to screen them. The total energy E_{es} consists of the following contributions:

$$E_{es} = E_{P,BTO} \times d_{BTO} + E_{P,SNO} \times d_{SNO} + E_d + E_{scr}. \quad (5)$$

Here, $E_{P,BTO}$ and $E_{P,SNO}$ are the energies needed to polarize the $BaTiO_3$ and $SmNiO_3$ slabs of respective thicknesses d_{BTO} and d_{SNO} [37,38], E_d is the electrostatic cost resulting from the imperfect screening of the interface charge σ_{inter} by the metallic electrons in the electrode [5,39] and E_{scr} is the cost associated with possible additional screening via electron-hole excitation across the $BaTiO_3$ band gap [37,38]. We describe the electrostatic model in more detail in Appendix B.

We estimate $E_{P,BTO}$ and $E_{P,SNO}$ from the energy profiles of bulk $BaTiO_3$ and $SmNiO_3$ (Fig. 8), obtained by displacing the atoms according to the lowest frequency polar phonon mode of the relaxed tetragonal structure with centrosymmetric symmetry and in-plane lattice constants strained to $SrTiO_3$. $BaTiO_3$ shows the characteristic double-well potential with energy minima at formal-charge polarization $\pm 24\,\mu C\,cm^{-2}$ (note that this value is slightly lower than the formal-charge polarization of the relaxed bulk). $SmNiO_3$ is lowest in energy at zero polar displacement, with the energy increasing particularly rapidly with polar displacements when rotations are active. This highlights again the importance of correctly treating the rotations in $SmNiO_3$.

1. Fit and extrapolation to larger slab thicknesses

We fit the model to our DFT calculations for $(BaTiO_3)_n(SmNiO_3)_4$ ($n = 5, 10, 30$) to extract the following three parameters: the band gap of $BaTiO_3$, the dielectric constant ϵ_r of $BaTiO_3$, and the effective metallic screening length λ_{fit}. The band gap linearly determines the energy cost of screening by electron-hole excitations (Eq. (B7)) and the energy of the depolarizing field is proportional to the ratio $\lambda_{fit}^2/\epsilon_r$ [Eq. (B5)]. We find good agreement for the shape of the energy profiles between DFT and the model for $\lambda_{fit}^2/\epsilon_r = 1 \times 10^{-19}\,m^2$ at the experimental band gap of 3.2 eV [40,41] (Fig. 12).

Note that the experimental band gap of 3.2 eV provides a better model fit to our DFT-calculated energy versus polarization for the superlattices than the DFT band gap of 1.8 eV, indicating a reduced need for electron-hole screening to describe the DFT calculations. This is because our use of formal charges to calculate the polarizations underestimates the polar discontinuity and hence the interfacial charge. It does not reflect a larger band gap in the DFT superlattice, for which the $BaTiO_3$ band gap is 1.8 and 1.7 eV with disabled and active $SmNiO_3$ rotations, respectively.

Here, we treat λ_{fit}/ϵ_r merely as a parameter, and we discuss its physical meaning as well as different ways to extract the

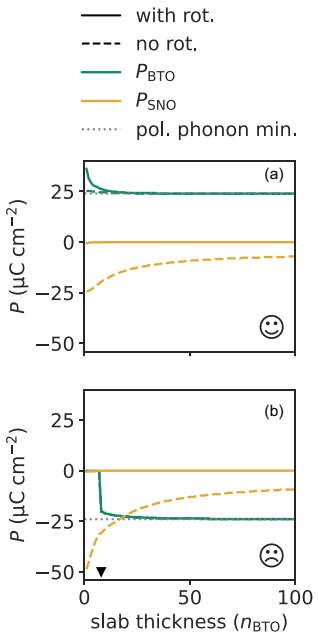

FIG. 9. Spontaneous polarization of the $BaTiO_3$ slab (green) and polar displacements of the $SmNiO_3$ slab (yellow) with active (full line) and disabled (dashed line) rotations in the $SmNiO_3$ as a function of slab thickness in formula units ($n_{BTO} = n_{SNO}$) as obtained from the electrostatic model. (a) Happy and (b) unhappy orientation of $BaTiO_3$ in the superlattice. The spontaneous polarization of bulk $BaTiO_3$ at 24.0 μC cm^{-2} obtained from freezing in the lowest-energy polar phonon displacements is shown as a comparison (dotted gray). The unhappy orientation has an energy minimum for 8 and more f.u. of $BaTiO_3$ (black triangle).

effective metallic screening length from the DFT calculations in the Appendix C.

Next, we use the model with the fitted parameters to calculate the evolution of the energy and spontaneous polarization of the happy and unhappy phases for larger slab thicknesses, and show the calculated energy profiles in Fig. 5 and the resulting spontaneous polarizations in Fig. 9. Figure 5 compares the energy profiles from DFT (a) with the results from the electrostatic model (b) for zero polar displacements in $SmNiO_3$. As imposed by the fit of $\lambda_{fit}^2/\epsilon_r$, a metastable minimum appears for the unhappy orientation between slab thicknesses of 5 and 10 formula units. Extending to thicker slabs in the electrostatic model, we see the two minima of the double well potential become closer in energy as thickness is increased until the energy differences between them are less than 15 meV/f.u. for 30 and negligibly small (∼1 meV/f.u.) for 100 layers of $BaTiO_3$. This is a result of the expected reduced influence of the polar discontinuity as the slab thickness is increased. Note that the depth of the energy well decreases with thickness compared to the DFT calculations in Fig. 5 because we keep the thickness of $SmNiO_3$ and $BaTiO_3$ equal whereas the $SmNiO_3$ thickness in the DFT calculations is kept at four layers and our normalization includes the number of formula units of both $BaTiO_3$ and $SmNiO_3$.

Figure 9(a) shows the corresponding size of the polar displacements for the happy orientation in superlattices of $BaTiO_3$ (green) and $SmNiO_3$ (yellow) with active (full line) and disabled (dashed line) rotations up to 100 layers. Not surprisingly, the polar displacement of $SmNiO_3$ with active rotations at one unit cell of $SmNiO_3$ is less than 1 μC cm^{-2} and disappears completely for thicker $SmNiO_3$ slabs. Consequently, the main compensation of the polar discontinuity comes from the $BaTiO_3$, with a spontaneous polarization of 36 μC cm^{-2} in a $BaTiO_3$ slab of one unit cell thickness. Note that this value is higher than the spontaneous polarization of bulk $BaTiO_3$, and that it reduces the remaining interface charge, to be screened by the metal and electron-hole excitations, to 13 μC cm^{-2}. For $SmNiO_3$ with disabled rotations, a considerable polar displacement in $SmNiO_3$ is present even for thick slabs. The polar displacement in $SmNiO_3$ reduces from 24 μC cm^{-2} at 1 f.u. to a value of 6 μC cm^{-2} at 100 f.u. while P_{BTO} is close to that of the soft mode minimum for all thicknesses. As previously observed in our DFT calculations, we do not see a critical thickness for the $BaTiO_3$ spontaneous polarization.

Since the unhappy orientation is not metastable up to seven layers, we see in Fig. 9(b) that the spontaneous polarization of $BaTiO_3$ remains zero up to this thickness. Once the unhappy orientation becomes metastable, P_{loc} jumps from zero to −20 μC cm^{-2} at eight $BaTiO_3$ layers, corresponding to the formation of the local minimum that we found within DFT. Interestingly, we see that the spontaneous polarizations of $BaTiO_3$ in superlattices with active and disabled rotations coincide. The additional polar displacements in $SmNiO_3$ with disabled rotations do not influence the thickness needed to form a metastable minimum even though the absence of rotations reduces the energy difference between the two polarization orientations (see Fig. 13). This apparently counterintuitive finding is a consequence of the fact that, in the unhappy orientation, any spontaneous polarization of $BaTiO_3$ increases the polar discontinuity. The formation of a metastable minimum is therefore only possible when the energy gain on polarizing $BaTiO_3$ exceeds the cost of increasing the polar discontinuity. In our model, both costs only depend on the $BaTiO_3$ and therefore, we observe the formation of a local minimum for the same slab thickness in superlattices with active and disabled $SmNiO_3$ rotations. The happy and unhappy orientations in Fig. 9 converge to the same absolute spontaneous polarization value for thick slabs, confirming that the unhappy orientation is less energetically disfavored for thick $BaTiO_3$.

2. *Influence of different parameters on the ferroelectric properties*

Next, we study the effect of varying the dielectric permittivity, the metallic screening, and the electron-hole excitations across the band gap on the ferroelectric properties of the $BaTiO_3$ layer. In particular, by changing the metallic screening, we are able to mimic a MIT in the electrode. For $\gamma = \frac{2\lambda_{fit}}{d_{BTO}}$ close to zero (small screening length) the electrode is a very good metal, at intermediate γ it is a poor metal and when $\gamma = 1$ we obtain the fully insulating state.

Figure 10 shows the calculated energy as a function of the $BaTiO_3$ spontaneous polarization across the MIT with $\gamma =$ 0.1 (yellow), 0.5 (purple), and 1 (black) for $\epsilon_r = 1$ (a), 30 (b) and 90 (c) and a slab thickness $d_{BTO} = d_{SNO} = 8$ unit cells. We compare the results with allowed (full line) and excluded

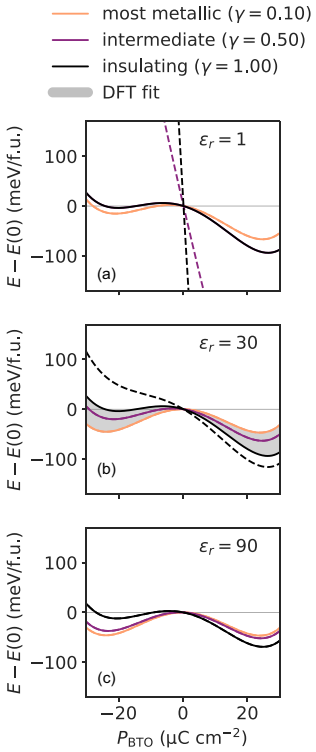

FIG. 10. Energy versus spontaneous polarization across the metal-to-insulator transition for (a) $\epsilon_r = 1$, (b) $\epsilon_r = 30$ and (c) $\epsilon_r = 90$ and slab thickness of $d = 8$ formula units for both $SmNiO_3$ and $BaTiO_3$. The MIT is mimicked by changing from a very short screening length $\gamma = 0.1$ ($\lambda_{\text{fit}} = 1.67$ Å) to a fully insulating system with $\gamma = 1$ ($\lambda_{\text{fit}} = 16.70$ Å). Results for models with allowed (full line) and forbidden (dashed line) electron-hole excitation across the band gap are shown. The polar displacements of $SmNiO_3$ are zero for all curves. For $\epsilon_r = 30$ (b), the range of energy values spanned by the values of λ, extracted from DFT using different methods, is superimposed in gray, with further details provided in Appendix C.

(dashed line) additional screening by electron-hole excitation across the $BaTiO_3$ band gap.

We can make the following conclusions from comparing the different plots: First, the additional carriers from electron-hole excitations strongly influence the stability of the unhappy orientation when the screening in the metal is poor and the dielectric permittivity in the ferroelectric is low. For low dielectric permittivities, the unhappy orientation is highly disfavored without screening by forming additional charge carriers (dashed line) in both the insulating and intermediate metallicity electrode cases. When the metallic screening is improved, fewer charge carrier excitations across the gap are needed and for the most metallic case, there are no electron-hole excitations present even at low ϵ_r. Second, a larger ϵ_r reduces the effect of the polar discontinuity and decreases the energy difference between the two polarization orientations. The double well of the insulating case (black) does not change much with ϵ_r, and the unhappy orientation is disfavored even for $\epsilon_r = 90$. For intermediate screening (purple), the double well potential is the most sensitive to ϵ_r. At $\epsilon_r = 1$, the intermediate screening and the most insulating cases (black) coincide while at $\epsilon_r = 90$, the intermediate screening is close to the most metallic case (yellow). For the most metallic case (yellow), the energy difference between the happy and unhappy orientation is negligible for $\epsilon_r = 90$, restoring the typical ferroelectric double well potential. Lastly, the energy difference between the happy and unhappy orientations increases for all cases as the system becomes more insulating, destabilizing the unhappy polarization orientation. For $\epsilon_r = 1$, neither the insulating nor intermediate metallicity electrodes can stabilize the unhappy orientation, and only the most metallic system (yellow curve) shows a metastable minimum. For $\epsilon_r = 30$, the intermediate screening leads to moderate stabilization of the unhappy orientation while a good screening significantly stabilizes the unhappy orientation. For $\epsilon_r = 90$, we again see that intermediate screening already results in the unhappy orientation being stable.

These results show that a change in the metallic screening length, as occurs across a MIT, can significantly alter the relative stabilities of the two $BaTiO_3$ polarization states. The changes in the ferroelectric double well potential across a MIT are most significant for higher dielectric susceptibilities and if the electrode has good screening in the metallic state. The destabilization of the unhappy orientation on changing from metallic to an insulating electrode found for $\epsilon_r = 90$ [Fig. 10(c)] could be significant enough to lead to switching from the unhappy to the happy orientation when the electrode changes from metallic to insulating.

In general, high ϵ_r and good metallic screening minimize the effects of the polar discontinuity on the ferroelectric. Thus if a metal with charged sublayers is to be used as a simple electrode, care should be taken to select one with those properties. Increasing the ferroelectric slab thickness additionally improves the switchability and reduces the impact of the polar discontinuity. To build a ferroelectric device that exploits the polar discontinuity, for example with a strong exchange bias, on the other hand, we recommend a low dielectric susceptibility and a metal with poor screening capability. Again, adjusting the film thickness controls the extent of the bias, with thinner $BaTiO_3$ films leading to unidirectional behavior.

To summarize this section, we find that the simple electrostatic model of Eq. (5) can reproduce the energy profiles over the range of thicknesses accessible in DFT calculations for thin films and can be conveniently used to extrapolate to larger slab thicknesses. We confirm that, as expected, the energy difference between happy and unhappy orientations is reduced in thicker films, becoming negligibly small for 30-formula-unit-thick $BaTiO_3$. In addition, our model allows us to test the effects of various parameters, such as the metallic screening length, on the properties of the superlattices, providing a simple and useful tool for studying how parameters such as slab thickness and metallic screening length affect the system's behavior. In particular, we find that the metallic screening length strongly influences the (meta)-stability of the unhappy $BaTiO_3$ orientation. This raises the interesting question of whether, in addition to the metallicity of the electrode affecting the spontaneous polarization of the ferroelectric, the reciprocal behavior might occur, and the orientation of the ferroelectric polarization might affect the metallicity of the electrode. We envisage a scenario in which the superlattice slab thicknesses and materials are selected so that the elec-

trode is insulating, and close to the metal-insulator transition when the ferroelectric is in its happy orientation. Switching the ferroelectric into its unhappy orientation could then force a transition of the electrode to the metallic state. Detailed electronic structure calculations for thicker slabs and at finite temperature would be helpful in identifying suitable material combinations and geometries.

IV. CONCLUSION

In summary, our DFT calculations confirm that the layer polarization in a metal can strongly affect the spontaneous polarization of the ferroelectric slab in metal-ferroelectric superlattices.

We showed that in $SmNiO_3/BaTiO_3$ superlattices the charge carriers in metallic $SmNiO_3$ cannot sufficiently screen its own layer polarization, and consequently, $BaTiO_3$ compensates for the polar discontinuity by orienting its spontaneous polarization parallel to the layer polarization of $SmNiO_3$. This out-of-plane spontaneous $BaTiO_3$ polarization stays stable down to a single unit cell, with no critical thickness for the ferroelectric thin films in this superlattice. Similarly to other systems with polar discontinuities [8,13], the unhappy direction which increases the polar discontinuity and the interface charge is highly disfavored and BTO thicknesses below ten layers do not even have a high energy metastable minimum for the unhappy direction. Based on the energy as a function of the soft mode distortion, we would expect the unhappy orientation to be metastable in thicker films.

We find that the inability of $SmNiO_3$ to fully screen the polar discontinuity is independent of whether its rotations are active or disabled. The lattice response is, however, different for the two cases and when the octahedral rotations are not taken into account, the ability of $SmNiO_3$ to form polar distortions is drastically overestimated.

We constructed an electrostatic model incorporating the energy lowering of polarizing the $BaTiO_3$ slab, the energy cost of forming polar displacements in $SmNiO_3$, the partial screening of the interfacial charges by the metallicity of the electrode, and the formation of additional screening charges by electron-hole excitation. The model reproduces our DFT behavior at low slab thicknesses and confirms that increasing the film thickness reduces the energy difference between the two polarization orientations. By varying our model parameters, we found that a shorter metallic screening length and a higher dielectric permittivity help to stabilize the unhappy orientation, indicating that a MIT could influence the ferroelectric switching behavior. This raises the question of whether, analogously, switching the ferroelectric could induce a MIT. If the ferroelectric is forced to the unhappy orientation with the electrode in its insulating state, the need to compensate the additional interface charges could drive the electrode to its metallic state, provided that it is close to the MIT temperature and the metallic screening length is short enough. Studying the influence of the polar discontinuity on the MIT could be an interesting direction for future research.

Using the model, we studied the influence of different model parameters on the ferroelectric double well potentials. We note that, while the model is useful for predicting general trends, there is a significant spread in realistic parameter values and quantitative results should be interpreted with caution.

In conclusion, ferroelectric switching can be controlled in novel ways when using an electrode that has a layer polarization with a ferroelectric with charge neutral layers. $SmNiO_3$ is particularly suitable as an electrode in ferroelectric devices when a strong exchange bias is desirable. The ferroelectric film thickness can be adjusted to control the extent of the bias, with thinner $BaTiO_3$ films leading to unidirectional behavior for easy switching of the ferroelectric, an electrode with no layer charges or with better metallic screening is recommended. If a good switching behavior is required with $SmNiO_3$ as an electrode, we recommend using a ferroelectric with a high dielectric constant or thick ferroelectric films. If the electrode also undergoes a MIT, this can lead to further exotic functionality.

We hope that our predictions inspire experimental work in these directions, both for fundamental research and for device applications.

ACKNOWLEDGMENTS

We thank M. Trassin and I. Efe for helpful discussions. This work was supported by the Swiss National Science Foundation under Grant No. 209454 and by ETH Zurich. The calculations for this work were performed on the ETH Zurich Euler cluster.

DATA AVAILABILITY

The relevant input files and data of our *ab initio* calculations are openly available on the Materials Cloud Archive [42] and the code needed for the data analysis and to reproduce the figures are available on github [43].

APPENDIX A: UNHAPPY ORIENTATION WITH DISABLED ROTATIONS

Figure 11 shows the unhappy orientation for the superlattice with disabled rotations. As for superlattices with active rotations, the three middle $BaTiO_3$ layers were fixed to the negative spontaneous-polarization value of bulk $BaTiO_3$. The response of the superlattice is analogous to the case with active rotations, the $SmNiO_3$ strongly increases its lattice response up to $32\,\mu C\,cm^{-2}$. while the $BaTiO_3$ interface layers reduce the ferroelectric displacements.

APPENDIX B: ELECTROSTATIC MODEL

The total electrostatic energy E_{es} per unit surface area of our system is given by

$$E_{es} = E_{P,BTO} \times d_{BTO} + E_{P,SNO} \times d_{SNO} + E_d + E_{scr}, \quad \text{(B1)}$$

where $E_{P,BTO}$ and $E_{P,SNO}$ are the energy per unit area of polarizing a slab of thickness d_{BTO} and d_{SNO}, respectively, E_d is the energy cost of the depolarizing field and E_{scr} the energy required to form screening charges by electron-hole excitation across the band gap [37,38]. The energy contribution needed

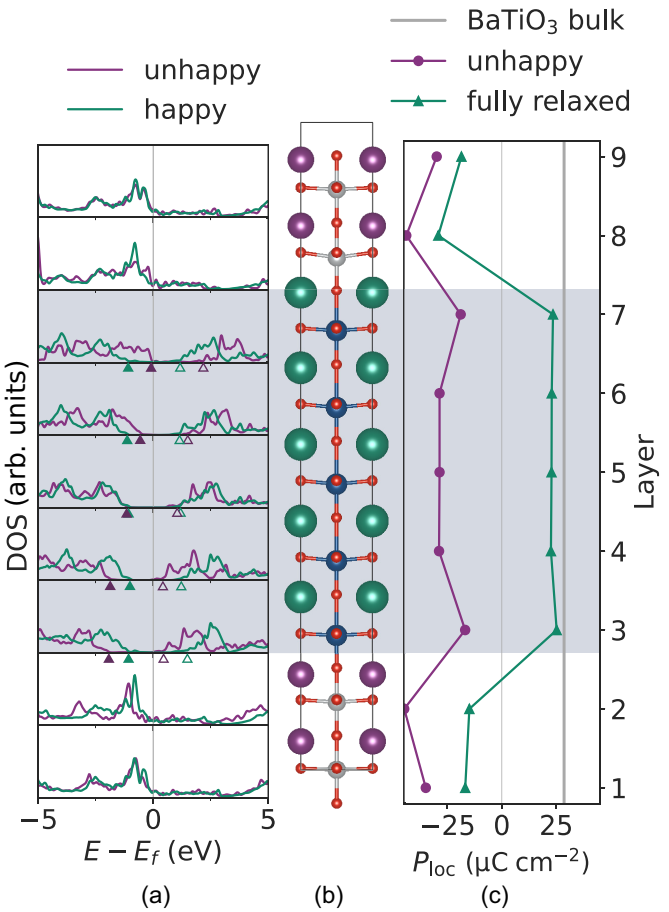

FIG. 11. Unhappy superlattice with three fixed $BaTiO_3$ layers and disabled rotations in $SmNiO_3$: (a) Local DOS of the happy superlattice from Fig. 2 (green) and superlattice with three $BaTiO_3$ layers fixed to the unhappy orientation (purple). The band shift in $BaTiO_3$ is indicated by corresponding green and purple triangles for the valence band maximum (full) and conduction band minimum (empty). (b) Superlattice after relaxation with three fixed layers. (c) Layer-resolved, local polarization (μC cm^{-2}) for relaxation with the fixed $BaTiO_3$ layers (purple) and for the relaxed happy structure from Fig. 2 (green).

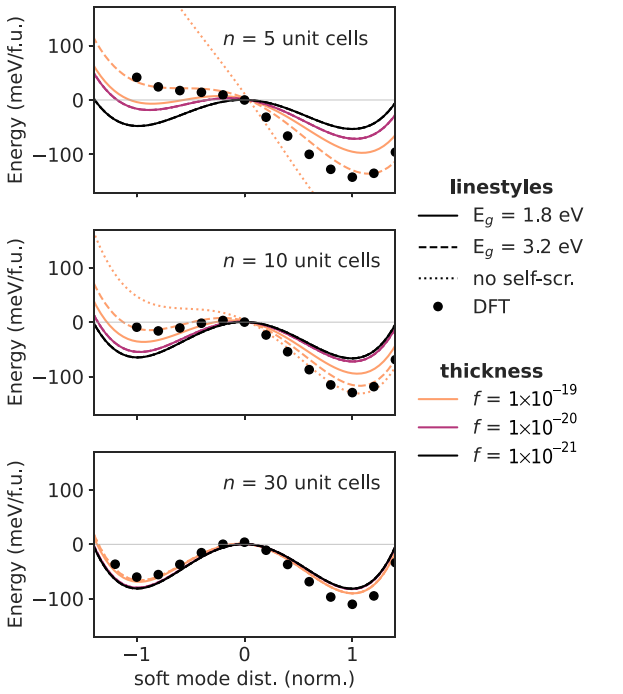

FIG. 12. Comparison of DFT results to the electrostatic model with different factors $\frac{\lambda^2}{\epsilon_r}$ and electronic band gaps $E_{\text{gap}} = 1.8\,\text{eV}$ (full line), 3.2 eV (dashed line) or no excitations across the band gap (dotted line). We show the energy divided by the total number of formula units in the superlattice as a function of the soft mode distortion of $BaTiO_3$ where -1 corresponds to the unhappy and 1 to the happy orientation and for $(BaTiO_3)_n(SmNiO_3)_4$ superlattices with $n = 5$, 10, or 30 unit cells.

to form polar displacements P is described by

$$E_{P,\text{ABO}} = aP_{\text{ABO}}^2 + bP_{\text{ABO}}^4, \tag{B2}$$

and we obtain a and b from fitting the curve to the energy profile obtained from modulating bulk $BaTiO_3$ and $SmNiO_3$ according to their lowest polar phonon mode. The calculated energy profiles are shown as the symbols in Fig. 8 and the a and b parameters of the fits (solid lines in Fig. 8) are given in Table I.

In contrast to Refs. [37,38], we have an interface to a conducting material. For an imperfect metal, the depolarizing field ε_d depends on the finite screening length λ following

$$\varepsilon_d \simeq -\frac{2\lambda\sigma_{\text{inter}}}{\epsilon_0\epsilon_r d_{\text{BTO}}}, \tag{B3}$$

where λ is the finite screening length, ϵ_0 is the dielectric constant in vacuum, ϵ_r is the relative permittivity of $BaTiO_3$, σ_{inter} is the interface charge from the different polarization contributions and d_{BTO} the ferroelectric film thickness [5]. This equation is valid for the case of $d_{\text{SNO}} \gg d_{\text{BTO}} \gg \lambda$ and short-circuit boundary conditions. Note that in the insulating case, the depolarizing field is given by [37,38]

$$\varepsilon_d = -\frac{\sigma_{\text{inter}}}{\epsilon_0\epsilon_r}, \tag{B4}$$

and we recover this field from Eq. (B3) when $\gamma = \frac{2\lambda}{d_{\text{BTO}}} = 1$. Simulating a metal-to-insulator transition in this model would correspond to varying γ from close to zero to a value of 1.

We obtain the electrostatic energy cost associated with the depolarizing field by integrating over the $BaTiO_3$ slab

TABLE I. Parameters (standard deviation in brackets) obtained from fitting Eq. (B2) to the DFT energies calculated as a function of the lowest polar phonon mode as shown in Fig. 8. Note that for $SmNiO_3$ with active rotations, the b parameter was set to zero to avoid an unphysical energy lowering outside the fit range.

Parameter	$BaTiO_3$	$SmNiO_3$	
		Rotations	No rotations
a (eV m^4 C^{-2})	−3.29 (27)	1034 (3)	−0.0200 (22)
b (eV m^8 C^{-4})	28.8 (3)	0	3.348 (20)

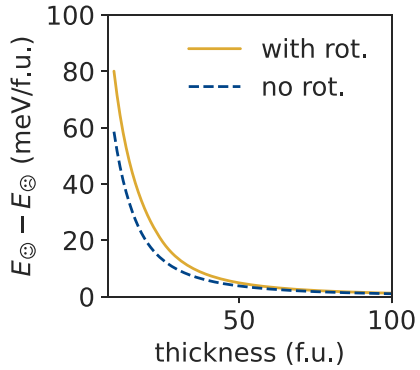

FIG. 13. Energy differences between happy and unhappy superlattices in the electrostatic model with active (yellow solid) and disabled (blue dashed) rotations for slab thicknesses from 8 to 100 $BaTiO_3$ and $SmNiO_3$ unit cells.

according to

$$E_d = \frac{\epsilon_0\epsilon_r}{2}\varepsilon_d^2 d_{\mathrm{BTO}} = \frac{2}{\epsilon_0\epsilon_r}\lambda^2\sigma_{\mathrm{inter}}^2\frac{1}{d_{\mathrm{BTO}}} = \frac{1}{2\epsilon_0\epsilon_r}\gamma^2\sigma_{\mathrm{inter}}^2 d_{\mathrm{BTO}}, \tag{B5}$$

and the total interface charge is calculated from the different polarization contributions and an additional screening contribution from electron-hole excitations σ_{scr} according to

$$\sigma_{\mathrm{inter}} = P_{\mathrm{layer}} - P_{\mathrm{BTO}} + P_{\mathrm{SNO}} - \sigma_{\mathrm{scr}}. \tag{B6}$$

The additional carriers σ_{scr} generated by electron-hole excitation across the band gap E_{gap} lead to a cost E_{scr} given by the relation [37,38]

$$E_{\mathrm{scr}} = \frac{\sigma_{\mathrm{scr}}}{e}E_{\mathrm{gap}}, \tag{B7}$$

where e is the electronic charge.

We determine if σ_{scr} is nonzero by finding the minimum of the total electrostatic energy according to

$$\frac{\partial E_{\mathrm{es}}}{\partial\sigma_{\mathrm{scr}}} = 0. \tag{B8}$$

Solving this equation for σ_{scr} we obtain the following condition:

$$\sigma_{\mathrm{scr}} = \begin{cases} 0 & \text{if } d_{\mathrm{BTO}} \leqslant \frac{\epsilon_0\epsilon_r}{\gamma^2}\frac{E_{\mathrm{gap}}}{e}\frac{1}{P_{\mathrm{tot}}} \\ P_{\mathrm{tot}} - \frac{\epsilon_r\epsilon_0}{\gamma^2}\frac{E_{\mathrm{gap}}}{e}\frac{1}{d_{\mathrm{BTO}}} & \text{if } d_{\mathrm{BTO}} > \frac{\epsilon_0\epsilon_r}{\gamma^2}\frac{E_{\mathrm{gap}}}{e}\frac{1}{P_{\mathrm{tot}}} \end{cases} \tag{B9}$$

with $P_{\mathrm{tot}} = P_{\mathrm{layer}} - P_{\mathrm{BTO}} + P_{\mathrm{SNO}}$.

We determine the unknown parameters E_{gap} and $\frac{\lambda^2}{\epsilon_r}$ by fitting to DFT calculations, see Fig. 12 and the respective values of 3.2 eV and $1 \times 10^{-19}\,\mathrm{m}^2$ best reproduce the DFT behavior. We obtain the spontaneous polarization that minimizes the total energy by calculating the energy landscape for a range of spontaneous polarization values and determining the global minimum. To model the unhappy orientation, we restrict the spontaneous polarization of $BaTiO_3$ to values of less than zero.

Figure 13 shows the energy difference between the local minimum for the happy and unhappy orientation as a function of the slab thickness. The energy of the unhappy orientation is higher overall for the superlattice with active rotations than one with disabled rotations even though both form a metastable for the unhappy orientation at the same slab thickness.

APPENDIX C: PHYSICAL RELEVANCE OF THE EFFECTIVE METALLIC SCREENING LENGTH

We extract the effective metallic screening length in four different ways from our DFT calculations. First, we estimate the screening length from the simplistic Thomas-Fermi model, which assumes that the electrons behave as a free-electron gas, and is given by

$$\lambda_{\mathrm{TF}} = \left(\frac{e^2}{\epsilon_0\epsilon_r}D(\varepsilon_{\mathrm{F}})\right)^{-1/2}, \tag{C1}$$

where $D(\varepsilon_{\mathrm{F}})$ is the DOS at the Fermi level, ε_{F}, and e is the electronic charge [44]. For our calculation of relaxed bulk $SmNiO_3$ with active rotations, we obtain $D(\varepsilon_{\mathrm{F}}) = 2.1 \times 10^{17}$ states/Å^3. In the most simple approach, we use $\epsilon_r = 1$ and we find a short screening length $\lambda_{\mathrm{TF}} = 0.4$ Å. Next, we include some of the ionic screening of the metal by using a relative permittivity bigger than one. For the DFT value of $\epsilon_r = 6$ [45], the screening length increases to 1.0 Å. We note that, for a correlated metal such as $SmNiO_3$, both these values are likely to be an underestimate, since the density of states in such systems tends to be high and the electrons rather localized and less able to contribute to screening than in the free-electron case.

Second, we convert the change in potential ΔV induced by the electric field across the $BaTiO_3$ slab to a screening length λ_{DOS} using the relation [39]

$$\lambda_{\mathrm{DOS}} = \frac{1}{2}\epsilon_0\epsilon_r\frac{\Delta V}{\sigma_{\mathrm{inter}}}. \tag{C2}$$

We extract ΔV from the $BaTiO_3$ core-state shift of the states between -29 and -24 eV in the DOS in a superlattice containing five layers of $BaTiO_3$ and four layers of $SmNiO_3$ frozen in their high-symmetry paraelectric atomic positions (Fig. 3) rather than from the step in the macroscopically averaged electrostatic potential used in previous studies [31,36,46]. When we set $\epsilon_r = 1$ in Eq. (C2), as was usually done in previous studies [5,31,36], we obtain $\lambda_{\mathrm{DOS}} = 0.2$ Å, and for the DFT value of $\epsilon_r = 6$ the corresponding screening length is 1.1 Å, resulting in similar screening lengths to the Thomas-Fermi level. As the slab calculation was performed with the ions frozen in their high-symmetry structures, these screening lengths still do not include effects from ionic screening beyond the dielectric permittivity.

Next, we can estimate λ_{fit} from the ratio $\lambda_{\mathrm{fit}}^2/\epsilon_r = 1 \times 10^{-19}\,\mathrm{m}^2$ obtained from fitting the electrostatic model. Here it is less clear what value to assume for ϵ_r. For $\epsilon_r = 1$, the ratio corresponds to $\lambda_{\mathrm{fit}} = 3.2$ Å, for the high frequency DFT value $\epsilon_r = 6$, it is 7.7 Å and for $\epsilon_r = 60$ (experimental literature values at room temperature vary between 60 and 110 [47–50]), we obtain a screening length of 24.5 Å.

This λ_{fit} is considerably larger again than the two previously extracted screening lengths λ_{DOS} and λ_{TF}, indicating that poor metallic screening in the model best reproduces the DFT behavior. The large λ_{fit} is likely a consequence of

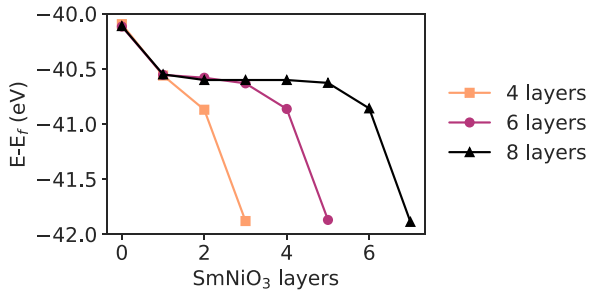

FIG. 14. Energy of $SmNiO_3$ core states for superlattices with five layers of $BaTiO_3$ and four (yellow), six (purple), and eight (black) layers of $SmNiO_3$.

the model capturing the high lattice response of the DFT calculations; we emphasize also that interfacial effects such as changes in chemical bonding at the interface are completely neglected in the model.

Lastly, we can estimate the metallic and ionic screening length by eye directly from the DOS. In Fig. 14 we show the location of the $SmNiO_3$ core states for superlattices with five layers of $BaTiO_3$ and varying $SmNiO_3$ layer thickness (4–6 layers). We see that the electronic states converge relatively quickly, within one layer at the lower SmO-TiO_2 interface and within two layers at the upper BaO-NiO_2 interface. We therefore obtain an electronic screening length of 1–2 formula units. Similarly, in Fig. 4, we see that the local polar displacements in $SmNiO_3$ (green line) relax within one formula unit to the bulk value (blue line), leaving us with an ionic screening length of one formula unit. Since one $SmNiO_3$ formula unit in the relaxed superlattices with active rotations is about 3.6 Å, we obtain screening lengths in between 3.6 and 7.2 Å. This screening length is in a similar range to the values obtained from the electrostatic model.

In Fig. 10, we show again the energy versus polarization of Fig. 5(b) for $\epsilon_r = 30$ and eight layers each of $SmNiO_3$ and $BaTiO_3$, superimposing in gray the physically plausible metallic screening range spanned by λ_{DOS} (low-energy limit) and λ_{fit} (high-energy limit). The wide range of values reasonably extracted from our DFT calculations suggests that the carrier screening in a complex oxide electrode might not be reliably captured in terms of a single screening length parameter. We conclude that these values should be treated with caution and considered as fitting parameters, without attributing too much physical significance to them.

[1] V. Garcia and M. Bibes, Ferroelectric tunnel junctions for information storage and processing, Nat. Commun. **5**, 4289 (2014).

[2] J. F. Scott, in *Ferroelectric Memories*, edited by K. Itoh and T. Sakurai, Springer Series in Advanced Microelectronics Vol. 3 (Springer, Berlin, 2000).

[3] C. A. F. Vaz, Y. J. Shin, M. Bibes, K. M. Rabe, F. J. Walker, and C. H. Ahn, Epitaxial ferroelectric interfacial devices, Appl. Phys. Rev. **8**, 041308 (2021).

[4] Y. Jiang, E. Parsonnet, A. Qualls, W. Zhao, S. Susarla, D. Pesquera, A. Dasgupta, M. Acharya, H. Zhang, T. Gosavi, C.-C. Lin, D. E. Nikonov, H. Li, I. A. Young, R. Ramesh, and L. W. Martin, Enabling ultra-low-voltage switching in $BaTiO_3$, Nat. Mater. **21**, 779 (2022).

[5] P. Chandra and P. B. Littlewood, A Landau primer for ferroelectrics, in *Physics of Ferroelectrics* (Springer, Berlin, 2007), Vol. 105, pp. 69–116.

[6] M. Stengel, Electrostatic stability of insulating surfaces: Theory and applications, Phys. Rev. B **84**, 205432 (2011).

[7] I. Efe, N. A. Spaldin, and C. Gattinoni, On the happiness of ferroelectric surfaces and its role in water dissociation: The example of bismuth ferrite, J. Chem. Phys. **154**, 024702 (2021).

[8] N. A. Spaldin, I. Efe, M. D. Rossell, and C. Gattinoni, Layer and spontaneous polarizations in perovskite oxides and their interplay in multiferroic bismuth ferrite, J. Chem. Phys. **154**, 154702 (2021).

[9] P. Yu, W. Luo, D. Yi, J. X. Zhang, M. D. Rossell, C.-H. Yang, L. You, G. Singh-Bhalla, S. Y. Yang, Q. He, Q. M. Ramasse, R. Erni, L. W. Martin, Y. H. Chu, S. T. Pantelides, S. J. Pennycook, and R. Ramesh, Interface control of bulk ferroelectric polarization, Proc. Natl. Acad. Sci. USA **109**, 9710 (2012).

[10] G. H. Kwei, A. C. Lawson, S. J. L. Billinge, and S. W. Cheong, Structures of the ferroelectric phases of barium titanate, J. Phys. Chem. **97**, 2368 (1993).

[11] J. Rodríguez-Carvajal, S. Rosenkranz, M. Medarde, P. Lacorre, M. T. Fernandez-Díaz, F. Fauth, and V. Trounov, Neutron-diffraction study of the magnetic and orbital ordering in $^{154}SmNiO_3$ and $^{153}EuNiO_3$, Phys. Rev. B **57**, 456 (1998).

[12] P. Lacorre, J. Torrance, J. Pannetier, A. Nazzal, P. Wang, and T. Huang, Synthesis, crystal structure, and properties of metallic $PrNiO_3$: Comparison with metallic $NdNiO_3$ and semiconducting $SmNiO_3$, J. Solid State Chem. **91**, 225 (1991).

[13] L. L. Tao and J. Wang, Ferroelectricity and tunneling electroresistance effect driven by asymmetric polar interfaces in all-oxide ferroelectric tunnel junctions, Appl. Phys. Lett. **108**, 062903 (2016).

[14] Y.-Z. Wu, H.-S. Lu, T.-Y. Cai, and S. Ju, Interface control of ferroelectricity in $LaNiO_3$-$BaTiO_3$ superlattices, AIP Adv. **4**, 087109 (2014).

[15] A. Malashevich, M. S. J. Marshall, C. Visani, A. S. Disa, H. Xu, F. J. Walker, C. H. Ahn, and S. Ismail-Beigi, Controlling mobility in perovskite oxides by ferroelectric modulation of atomic-scale interface structure, Nano Lett. **18**, 573 (2018).

[16] G. Kresse and J. Furthmüller, Efficiency of *ab initio* total energy calculations for metals and semiconductors using a plane-wave basis set, Comput. Mater. Sci. **6**, 15 (1996).

[17] G. Kresse and J. Furthmüller, Efficient iterative schemes for *ab initio* total-energy calculations using a plane-wave basis set, Phys. Rev. B **54**, 11169 (1996).

[18] J. P. Perdew, A. Ruzsinszky, G. I. Csonka, O. A. Vydrov, G. E. Scuseria, L. A. Constantin, X. Zhou, and K. Burke, Restoring the density-gradient expansion for exchange in solids and surfaces, Phys. Rev. Lett. **100**, 136406 (2008).

[19] P. E. Blöchl, Projector augmented-wave method, Phys. Rev. B **50**, 17953 (1994).

[20] G. Kresse and D. Joubert, From ultrasoft pseudopotentials to the projector augmented-wave method, Phys. Rev. B **59**, 1758 (1999).

[21] J. J. Peng, C. Song, B. Cui, F. Li, H. J. Mao, G. Y. Wang, and F. Pan, Manipulation of orbital occupancy by ferroelectric polarization in $LaNiO_3/BaTiO_{3-\delta}$ heterostructures, Appl. Phys. Lett. **107**, 182904 (2015).

[22] R. Wahl, D. Vogtenhuber, and G. Kresse, $SrTiO_3$ and $BaTiO_3$ revisited using the projector augmented wave method: Performance of hybrid and semilocal functionals, Phys. Rev. B **78**, 104116 (2008).

[23] H. J. Monkhorst and J. D. Pack, Special points for Brillouin-zone integrations, Phys. Rev. B **13**, 5188 (1976).

[24] R. Resta, Macroscopic electric polarization as a geometric quantum phase, EPL **22**, 133 (1993).

[25] R. D. King-Smith and D. Vanderbilt, Theory of polarization of crystalline solids, Phys. Rev. B **47**, 1651 (1993).

[26] A. Ganose, J. Riebesell, J. George, J. Shen, A. S. Rosen, A. A. Naik, nwinner, M. Wen, rdguha1995, M. Kuner, G. Petretto, M. Horton, Z. Zhu, H. Sahasrabuddhe, A. Kaplan, J. Schmidt, C. Ertural, R. Kingsbury, M. McDermott, R. Goodall, T. Purcell, A. Bonkowski, D. Zügner, and J. Qi, Materialsproject/atomate2: v0.1.14, Zenodo (2024), doi: 10.5281/zenodo.10677080.

[27] A. Togo, First-principles phonon calculations with phonopy and phono3py, J. Phys. Soc. Jpn. **92**, 012001 (2023).

[28] A. Togo, L. Chaput, T. Tadano, and I. Tanaka, Implementation strategies in phonopy and phono3py, J. Phys.: Condens. Matter **35**, 353001 (2023).

[29] Y.-H. Tang and M.-H. Tsai, Ferroelectric properties of nanometer-scale barium titanate films from first principles, J. Appl. Phys. **103**, 034305 (2008).

[30] M. S. J. Marshall, A. Malashevich, A. S. Disa, M.-G. Han, H. Chen, Y. Zhu, S. Ismail-Beigi, F. J. Walker, and C. H. Ahn, Conduction at a ferroelectric interface, Phys. Rev. Appl. **2**, 051001(R) (2014).

[31] G. Gerra, A. K. Tagantsev, N. Setter, and K. Parlinski, Ionic polarizability of conductive metal oxides and critical thickness for ferroelectricity in $BaTiO_3$, Phys. Rev. Lett. **96**, 107603 (2006).

[32] X. Liu, Y. Wang, P. V. Lukashev, J. D. Burton, and E. Y. Tsymbal, Interface dipole effect on thin film ferroelectric stability: First-principles and phenomenological modeling, Phys. Rev. B **85**, 125407 (2012).

[33] D. I. Bilc and D. J. Singh, Frustration of tilts and A -site driven ferroelectricity in $KNbO_3$-$LiNbO_3$ alloys, Phys. Rev. Lett. **96**, 147602 (2006).

[34] T. H. Kim, D. Puggioni, Y. Yuan, L. Xie, H. Zhou, N. Campbell, P. J. Ryan, Y. Choi, J.-W. Kim, J. R. Patzner, S. Ryu, J. P. Podkaminer, J. Irwin, Y. Ma, C. J. Fennie, M. S. Rzchowski, X. Q. Pan, V. Gopalan, J. M. Rondinelli, and C. B. Eom, Polar metals by geometric design, Nature (London) **533**, 68 (2016).

[35] N. A. Benedek and C. J. Fennie, Why are there so few perovskite ferroelectrics? J. Phys. Chem. C **117**, 13339 (2013).

[36] J. Junquera and P. Ghosez, Critical thickness for ferroelectricity in perovskite ultrathin films, Nature (London) **422**, 506 (2003).

[37] C. Gattinoni and N. A. Spaldin, Prediction of a strong polarizing field in thin film paraelectrics, Phys. Rev. Res. **4**, L032020 (2022).

[38] J. A. Mundy, B. F. Grosso, C. A. Heikes, D. Ferenc Segedin, Z. Wang, Y.-T. Shao, C. Dai, B. H. Goodge, Q. N. Meier, C. T. Nelson, B. Prasad, F. Xue, S. Ganschow, D. A. Muller, L. F. Kourkoutis, L.-Q. Chen, W. D. Ratcliff, N. A. Spaldin, R. Ramesh, and D. G. Schlom, Liberating a hidden antiferroelectric phase with interfacial electrostatic engineering, Sci. Adv. **8**, eabg5860 (2022).

[39] C. Lichtensteiger, M. Dawber, and J.-M. Triscone, Ferroelectric size effects, in *Physics of Ferroelectrics* (Springer, Berlin, 2007), Vol. 105, pp. 305–338.

[40] S. H. Wemple, Polarization fluctuations and the optical-absorption edge in $BaTiO_3$, Phys. Rev. B **2**, 2679 (1970).

[41] J. Nowotny and M. Rekas, Defect structure, electrical properties and transport in barium titanate. III. Electrical conductivity, thermopower and transport in single crystalline $BaTiO_3$, Ceram. Int. **20**, 225 (1994).

[42] E. Simmen and N. A. Spaldin, Interplay of metallicity, ferroelectricity and layer charges in $SmNiO_3/BaTiO_3$ superlattices, Mater. Cloud Archive **2025.54** (2025).

[43] https://github.com/materialstheory/metSNO-BTO-superlattices.

[44] C. Kittel, *Introduction to Solid State Physics*, 8th ed. (Wiley, Hoboken, NJ, 2005).

[45] P. Ghosez, First-principles study of the dielectric and dynamical properties of barium titanate, Ph.D. thesis, Université catholique de Louvain, Louvain-la-Neuve, 1997.

[46] A. Baldereschi, S. Baroni, and R. Resta, Band offsets in lattice-matched heterojunctions: A model and first-principles calculations for GaAs/AlAs, Phys. Rev. Lett. **61**, 734 (1988).

[47] A. V. Turik and N. B. Shevchenko, Dielectric spectrum of $BaTiO_3$ single crystals, Physica Status Solidi B **95**, 585 (1979).

[48] D. Berlincourt and H. Jaffe, Elastic and piezoelectric coefficients of single-crystal barium titanate, Phys. Rev. **111**, 143 (1958).

[49] M. Zgonik, P. Bernasconi, M. Duelli, R. Schlesser, P. Günter, M. H. Garrett, D. Rytz, Y. Zhu, and X. Wu, Dielectric, elastic, piezoelectric, electro-optic, and elasto-optic tensors of $BaTiO_3$ crystals, Phys. Rev. B **50**, 5941 (1994).

[50] O. Nakao, K. Tomomatsu, S. Ajimura, A. Kurosaka, and H. Tominaga, Influence of 180° domains on ferroelectric properties of $BaTiO_3$ single crystal, Appl. Phys. Lett. **61**, 1730 (1992).